Published in final edited form as:
Biochemistry. 2010 October 5; 49(39): 8636–8645. doi:10.1021/bi101106x.

Positions 94–98 of the lactose repressor N-subdomain monomer•monomer interface are critical for allosteric communication†

Hongli Zhan§, **Maricela Camargo**, and **Kathleen S. Matthews***
Department of Biochemistry and Cell Biology, Rice University MS-140, 6100 S. Main, Houston, Texas 77005

Abstract

The central region of the LacI N-subdomain monomer•monomer interface includes residues K84, V94, V95, V96, S97, and M98. The side chains of these residues line the β-strands at this interface and interact to create a network of hydrophobic, charged, and polar interactions that significantly rearranges in different functional states of LacI. Prior work showed that converting K84 to an apolar residue or converting V96 to an acidic residue impedes the allosteric response to inducer. Thus, we postulated that a disproportionate number of substitutions in this region of the monomer•monomer interface would alter the complex features of the LacI allosteric response. To explore this hypothesis, acidic, basic, polar, and apolar mutations were introduced at positions 94–98. Despite their varied locations along the β-strands that flank the interface, ~70% of the mutations impact allosteric behavior, with the most significant effects found for charged substitutions. Of note, many of the LacI variants with minor functional impact exhibited altered stability to urea denaturation. The results confirm the critical role of amino acids 94–98 and indicate that this N-subdomain interface forms a primary pathway in LacI allosteric response.

Keywords

LacI; allostery; conformational change; ligand binding; structure/function

The lactose repressor protein (LacI1) has served as a model for gene regulation, allosteric behavior, and protein folding (1–4). In this study, we utilize this genetic regulatory protein to examine the role of residues that line a subunit interface and sustain significant change during the LacI allosteric response to inducer binding. LacI accomplishes transcription repression by binding its DNA recognition site, the operator, and inhibits RNA polymerase transcription of the associated genes. In the presence of inducer (either the gratuitous inducer, IPTG, or the natural inducer, allolactose), the protein undergoes an allosteric conformational change that diminishes affinity for the operator sequence, thus allowing transcription of the *lac* structural genes (1–4).

The LacI functional unit is the dimer, with one operator DNA-binding site per dimer and one inducer-binding pocket per monomer. Structurally, the LacI monomer can be divided

†This work was supported by Robert A. Welch Grant C-576 and NIH Grant GM22441 to KSM.

*To whom correspondence should be addressed, Telephone: 713-348-4871, FAX: 713-348-2750, ksm@rice.edu .
§Present address: Department of Molecular and Human Genetics, Mail Stop NAB 2015, Baylor College of Medicine, One Baylor Plaza, Houston, Texas 77030

[1]Abbreviations: LacI, lactose repressor protein; IPTG, isopropyl-β,D-thiogalactoside; ONPF, o-nitrophenyl-β,Dfucopyranoside; TMD, targeted molecular dynamics.

into five regions (Figure 1A). Within a dimer, the N-subdomains form a critical monomer•monomer interface that differs significantly between the operator- and inducer-bound forms (5–7) (Figure 1B). In addition, each N-subdomain forms the top half of an inducer-binding site, which is sandwiched on the bottom by the C-subdomain (5, 7). The dimeric functional units are connected through the C-terminal 4-helical bundle (5, 8).

In the operator-bound state of LacI (Figure 1B, left), myriad interactions are formed by side chains within the monomer•monomer interface, including lysine at 84, valines at 94, 95, and 96, serine at 97, and methionine at 98 (6, 9). A striking feature is that the charged side chains of K84 are buried in the otherwise apolar interface in the DNA-bound structure. The buried K84 side chains engage with a solvent anion and the main chain at V94 and V96', are sandwiched between hydrophobic groups, and appear as dual wedges separating the two flanking β-sheets (5, 6). The apolar region of the K84 side chain contacts V96' and M98' in the partner subunit (6, 9, 10).

This interface changes significantly in different functional states. In the structure of LacI bound to inducer, K84 moves out of the interface to become more solvent-exposed and interacts with the side chain of E100'; the β-strands move closer to form a continuous sheet through the two N-subdomains (Figure 1B, right) (6, 9, 10). In the intermediate state of a targeted molecular dynamics (TMD) simulation of the allosteric change (11), one K84 side chain has moved out of the interface (designated in larger font, Figure 1B middle), whereas the other (K84') stays within the interface. This toggle-like movement of K84 appears to be a key feature of the allosteric transition that aligns the hinge helices for interaction with operator DNA in the absence of inducer, and the arrangement of this interface strongly correlates to the conformational state of the repressor (10, 12, 13).

Apolar substitutions in this interface are known to affect allosteric behavior. Replacing the charged side chain at position 84 with apolar residues significantly alters LacI function. The variants K84A and K84L diminish the effect of inducer binding on DNA binding affinity, significantly decrease the rate (but not equilibrium) constants for inducer binding, and highly stabilize the protein to urea denaturation (13–15). The variant A81V greatly decreases operator affinity and abolishes allosteric response to inducer, presumably through fixing LacI in the “inducer-bound” conformation (16). Biphasic inducer binding was observed for S77L (17). A81V and S77L increase the hydrophobicity of the N-subdomain interface near the inducer-binding site and potentially impact the movement of the β-sheets required for the allosteric response.

Here, we explore further the allosteric contribution of individual amino acid side chains in this region by introducing substitutions at positions 94, 95, 96, 97, and 98 on the flanking β-sheets and examining multiple parameters of function. The pattern of results is not strictly related to position, as might have been anticipated by the alternate orientation of residues along the β-sheet structures. The most substantial and pervasive functional impact is on release of operator DNA in response to inducer binding, which correlates most strongly to the introduction of charge, either positive or negative. These results confirm the role of this region in allosteric response and further illuminate the important functional contribution of the web of interactions at this N-subdomain interface.

MATERIALS AND METHODS

Plasmids and Mutagenesis

Using the pLS1 plasmid containing the LacI gene, mutations were introduced by PCR mutagenesis using site-specific primers (Quickchange, Stratagene, La Jolla, CA) (18,19), and the PCR product was exposed to *Dpn*I to digest template DNA. Following plasmid

amplification in either XL1-blue or DH5α cells, the entire LacI coding region of each mutant plasmid was sequenced by SeqWright Inc. (Houston, TX) to confirm that no mutations were identified other than those intended.

Purification

For LacI variant expression, the corresponding plasmid was transformed into *E. coli* BLIM cells (18). After growth in 5 ml and then 50 ml cultures, the BLIM cells were transferred to twelve 1 L cultures of 2 × YT media and kept at 37°C with shaking for 20 hr. The cells were harvested by centrifugation and then resuspended in breaking buffer (200 mM Tris-HCl, pH 7.6, 200 mM KCl, 5% glucose, 10 mM magnesium acetate, and 0.3 mM DTT). This cell paste was frozen at –20°C with addition of a small amount of lysozyme (~0.5 mg/ml). Protein purification was performed as described previously (12). Protein purity was confirmed by SDS-PAGE and was generally >95%. Each purified protein solution was divided into aliquots and stored at –80°C. Protein activity was monitored by DNA activity assays using a concentration of radiolabeled DNA at least 10-fold above the K_d for DNA binding and was generally >90%.

DNA binding

Nitrocellulose filter binding assays were used to measure DNA binding affinities of LacI mutants (20,21). The two strands of the 40-base pair wild-type operator O^1 sequence (5'-TGTTGTGTGGAATTGTGAGCGGATAACAATTTCACACAGG-3') (22) were purchased separately from Biosource International (Camarillo, CA). These strands were hybridized in polynucleotide kinase buffer (70 mM Tris-HCl, pH 7.6, 10 mM $MgCl_2$, 5 mM DTT) and radiolabeled with polynuceleotide kinase at the 5'-end using [γ-^{32}P]ATP. Any remaining free nucleotide was removed by a Nick column (Amersham Biosciences, Uppsala, Sweden). For affinity assays, DNA concentration was at least 10-fold below the K_d for operator binding, and protein concentration was varied as indicated. For assays in the presence of inducer, IPTG concentration was 1 mM. The reaction mixtures were incubated for 20–30 min and filtered through nitrocellulose (Schleicher and Schuell, Keene, NH or Whatman, Florham Park, NJ) to capture protein-DNA complex and allow free DNA to pass through the filter. After exposure to a phosphorimaging plate overnight, the retained protein-bound, radiolabeled DNA was detected and quantified using a Fuji phosphorimager. Data (Y_{obs}) were analyzed using IgorPro (Wavemetrics, CA) to estimate values for the variables in the following equation:

$$Y_{\text{obs}} = Y_{\max} * \frac{[\text{LacI}]^n}{K_d{}^n + [\text{LacI}]^n} + c \quad (1)$$

where Y_{obs} is the retained radiolabel at different protein concentrations, $Y_{\max}$ is the maximal radioactivity retained; K_d is the apparent dissociation constant; c is background radioactivity; and n is the Hill coefficient. The value of n was found to cluster around 1, as expected for DNA binding.

IPTG binding

Inducer binding elicits a shift in the fluorescence emission maximum toward higher wavelengths (23). Thus, inducer binding affinity of LacI mutants was monitored using total fluorescence emission intensity change at wavelengths greater than 340 nm. Fluorescence spectra with excitation at 285 nm were collected from 300 to 380 nm. For accurate measurement, the protein concentration was set ~10-fold below the wild-type LacI K_d for inducer binding, 1.5×10^{-7} M in monomer, and IPTG concentration was varied. Data were

analyzed using the following equation on the program Igor Pro (Wavemetrics, CA) to accommodate the fluorescence signal decrease as IPTG binds:

$$Y_{obs}=Y_{max}-\left(Y_{max}*\frac{[IPTG]^n}{K_d^n+[IPTG]^n}\right)+c \quad (2)$$

Y_{obs} corresponds to the fluorescence at a specific IPTG concentration; Y_{max} is the total fluorescence signal change in response IPTG binding; n is the Hill coefficient for IPTG binding; K_d is the apparent equilibrium dissociation constant; and c is the fluorescence signal in the presence of a saturating concentration of IPTG. These data were used in calculating the fraction protein bound by IPTG.

Operator release

To determine the extent of release, the protein was first incubated with operator to form the LacI•DNA complex. Increasing concentrations of IPTG were then added to release operator from the preformed LacI•DNA complex. For these experiments, the concentration of radiolabeled DNA was 1.5×10^{-12} M, the repressor concentration was set to obtain ~80–90% saturation of protein by operator DNA (13,24), and the concentration of inducing sugar was varied as shown. A Fuji phosphorimager was utilized to measure radiolabel intensity, and the data were analyzed with equation 2 by replacing K_d with $[IPTG]_{mid}$. This value is for comparative purposes only, since operator release involves (at a minimum) the binding of inducer molecules and the accompanying protein conformational change leading to operator release. Therefore, the $[IPTG]_{mid}$ value is not an equilibrium constant and can only be used as a means to compare the properties of different proteins. The protein concentrations used in the operator release experiments were as follows: wild-type LacI, 2.4×10^{-10} M; V94K, 7.5×10^{-11} M; V94L, 1.9×10^{-10} M; V94T, 5×10^{-11} M; V95D, 1.3×10^{-10} M; V95K, 5.8×10^{-11} M; V95L, 8×10^{-10} M; V95T, 2.5×10^{-11} M; V96K, 1×10^{-8} M; V96L, 6×10^{-11} M; V96T, 2×10^{-10} M; S97E, 4.5×10^{-11} M; S97K, 8×10^{-11} M; S97L, 7.6×10^{-11} M; M98E, 2.2×10^{-10} M; M98I, 5×10^{-10} M; and M98K, 1×10^{-9} M.

Urea denaturation

Urea denaturation experiments were performed by monitoring changes in tryptophan fluorescence intensity at 340 nm, and, in a few cases, the data were confirmed by circular dichroism. The protein was mixed with varying concentrations of urea (made fresh daily) (25,26) and incubated for 2 hr at room temperature. Protein concentration was 2×10^{-6} M in monomer. To ensure that equilibrium was obtained, varying incubation times were employed. The concentration of urea was confirmed by refractometry (27,28). Data were analyzed according to previous authors (28,29) to determine $\Delta G°_{N\text{-}U}$ and m values. Note that these analyses presume only two states (native and unfolded) are present in the transition region and that the reaction is reversible. Although previous work has demonstrated that these presumptions apply to wild-type LacI, fluorescence and CD both monitor unfolding to a tetramer tethered at the C-terminus (25). Nonetheless, we note here that differences may arise in the mutant proteins that do not meet the assumptions of this analysis, although the data do not indicate an obvious violation of these assumptions. Replicate denaturation curves for each protein were used in a global fit to minimize the errors in data analyses.

Pymol analysis

The mutagenesis function in the program Pymol (http://pymol.sourceforge.net) was used to create models of the subunit interface in different conformations for selected mutations. Pymol offers a simple annealing simulation to avoid potential steric clashes, allowing an

examination of the impact on structure at the interface. In cases where multiple configurations arose, the model with the higher probability was utilized.

RESULTS

Generation of mutants and protein purification

The significant structural changes observed for the 94–98 region in response to IPTG binding (5,6,9–13) led us to postulate that a disproportionate set of substitutions in this region would alter allosteric response. In order to explore the role of positions 94–98 in LacI allosteric response, apolar, polar, and charged residues were introduced for V94 (K, L, T), V95 (D, K, L, T), V96 (K, L, T), S97 (E, K, L), and M98 (E, I, K) on the two flanking β-sheets that form a central portion of the N-subdomain subunit interface. Residues were selected to complement previous data,2 to determine impact of additional apolar moities (L or I), to test the influence of charge (D, E, or K), or to measure consequences of a potential hydrogen bond (T). Mutant proteins purified in a manner similar to tetrameric wild-type protein, indicating that they have similar oligomeric states.

Measuring Basic Function: Binding Operator DNA and Inducer

We first verified that the interface mutants are capable of both operator DNA and inducer binding. From this perspective, most substitutions were relatively benign. Nitrocellulose filter binding assays were employed to determine operator O^1 binding affinity (reported as dissociation constant, $K_{R/O}$) of individual mutant proteins (Figure 2 and Table 1) (13,20,21). In the absence of inducer, ~70% of these mutant proteins bind O^1 similarly to wild-type protein, with affinities that are within 3-fold of that for LacI. The variants V95L, M98E, M98I, and M98K exhibited ~5- to 15-fold lower affinity for operator DNA, whereas operator binding was substantially decreased for V96K (~60-fold). V95K and S97E may have slightly enhanced operator-binding affinities.

Inducer binding (reported as dissociation constant, $K_{R/I}$) can be monitored directly by fluorescence titration (13,20,23), and the results for interface variants are shown in Figure 3 and Table 2. Only V96T, S97E and S97K exhibit significantly lower inducer-binding affinities compared to wild-type LacI. Intriguingly, M98E exhibits biphasic inducer binding, with wild- type affinity for the first inducer binding event and a significantly decreased affinity for the second. Biphasic inducer binding has been observed previously in S77L (17), which impacts a region at the N-subdomain interface very near the inducer-binding site and exhibits properties suggesting an impeded conformational change. The remaining interface variants are within ~3-fold of wild-type LacI affinity.

Quantification of Allosteric Function

With fundamental binding properties largely intact for this set of mutants, the next step was to measure allosteric properties in two different ways. First, we determined the K_d value for operator binding in the presence of IPTG ($K_{RI/O}$) for comparison to the value in the absence of IPTG previously measured ($K_{R/O}$, see above) and derived the ratio between these values, which we have termed “allosteric amplitude” (Table 1, columns 3 and 4). For wild-type LacI, IPTG binding decreases operator binding affinity by >1000-fold (Table 1), corresponding to an allosteric amplitude of >1000. Second, we determined the midpoint concentration of IPTG ($[IPTG]_{mid}$) required for operator release and the extent of release (Table 2, columns 2 and 4). For wild-type LacI, $[IPTG]_{mid}$ is very similar to the K_d for IPTG binding in the absence of DNA, which has been interpreted to indicate that two IPTG

[2]A previous study explored the impact of substituting acidic and amide residues (D, E, Q, N) for V94 and V96 (12). The results of this study and results for K84A/K84L (13–15) are included in the comprehensive analysis shown in Table 4.

molecules are required to bind a dimer in order to effect the complete allosteric change (13). The extent of operator release is closely related to the allosteric amplitude. If the latter is much diminished, so that some fraction of DNA remains bound to the LacI-IPTG complex, then the extent of release must also be diminished. It is important to note that all of these parameters are intimately linked, and measurement of a variety of functional effects is essential in assessing the impact of substitutions on allosteric response.

Impact of Inducer on Operator Binding and Correlation with Phenotype

Half of the mutant proteins – V95D, V95K, V96K, V96L, S97E, S97K, M98E, and M98K – have significantly increased affinities for binding operator DNA in the presence of inducer (Figure 2, Table 1), corresponding to a decrease in allosteric amplitude. Overall, the observed operator binding behavior and response to inducer align reasonably well with the phenotypes previously identified for each of these substitutions (Table 1) (30). The discrepancy between wild-type DNA binding affinity and "−" phenotype for V94K may correlate with its significantly low protein expression level and instability (>50-fold lower yield and significantly lower stability than wild-type protein, see below). The lower DNA binding affinity for V96K would be expected to yield a "−" phenotype, in contrast to the observed "+" analysis for this variant (30); the origin of this difference is unclear.

Monitoring Operator Release as a Function of IPTG Concentration

"Operator release" experiments with varied IPTG concentrations quantitatively assess allostery by determining (1) how much inducer is required to release operator ($[IPTG]_{mid}$) and (2) the extent of the LacI-bound operator that is released. Operator release experiments were performed using the nitrocellulose filter binding assay (13,20), and the results are presented in Figure 4 and Table 2 (columns 2 and 4). The mutants V96T, S97E, S97K, and M98E require >5-fold more IPTG to release operator. The extent of release is significantly lower for V95K, V96K, S97E, S97K, M98E, and M98K. Note that all six of the latter mutations introduce charged side chains, and four of these six variants bring an additional lysine residue into this complex interface.

These operator release experiments involve a *minimum* of two events: inducer binding and conformational change to release operator. The measured $[IPTG]_{mid}$ thus contains combined information from at least these two processes. Comparing the K_d for repressor•IPTG with $[IPTG]_{mid}$ provides an "induction ratio" (Table 2) to take into account diminished inducer binding. When altered IPTG binding is factored out of $[IPTG]_{mid}$ in this manner, values for V94K, V95D, and V95K remain 2 to 5-fold greater than that for wild-type LacI, indicating significant changes in their allosteric response. Interestingly, the mid-point of operator release corresponds to the K_d of the second inducer binding event for M98E. This result is consistent with previous conclusions that two IPTG molecules must bind a dimer to effect the full allosteric response (13,32).

Stability of the interface mutants

Side chain variation within the N-subdomain interface alters the overall hydrophobic/charge relationship and can therefore affect protein stability, as observed for K84A and K84L (15). The results of urea denaturation experiments are shown in Figure 5 and Table 3. Interestingly, urea unfolding is unaffected in approximately half of the LacI variants in this study, and two of the proteins exhibit slightly enhanced stability. The remaining mutant proteins exhibit lower or significantly lower stability. The most important factor contributing to significant destabilization appears to be positive charge, presumably due to charge repulsion with K84 (*e.g.*, V94K, V96K). Moderate destabilization appears due to enhanced bulk, increased polarity, or charge (*e.g.*, V94L, V94T, V95D, S97L, M98K).

DISCUSSION

The underlying hypothesis for these experiments was that alterations along the N-subdomain monomer•monomer interface defined by LacI residues 94–98 would significantly impact allosteric behavior. This hypothesis was based on: (1) structural differences in this region between LacI•ONPF•operator DNA and LacI•IPTG (5–7,9,10), (2) the results of targeted molecular dynamics simulation that indicated a central role for this region in propagation of the allosteric signal from the IPTG site to the DNA site (11), (3) data from prior studies that have targeted residues in this area (12–15), and (4) network and computational analyses that indicate an allosteric role for this interface (10,33).

The results obtained demonstrate that this region is a critical element in LacI allosteric response. Examining the entire cadre of mutants in this interface,[2] 18 of the 26 variants altered some feature of allosteric behavior. Of these, 11 introduced charged substitutions, 4 substituted polar for apolar residues, and 3 enhanced apolar character. Thus, effects on allosteric function correlate most strongly with the introduction of charge (both positive and negative) and are largely unrelated to position. The strongest correlation with position was for stability to urea denaturation, with positions 94 and 96 accounting for 11 of the 17 variants with alterations in stability. Below we group the mutations based on their functional impact and then place this information in a larger context of allosteric behavior.

Analysis by functional similarity and modeling of LacI variant structures

To understand these collective measurements, we have grouped the mutants based on common properties (Table 4). For this analysis, we included prior results for acidic and amide substitutions at positions V94 and V96 (12) and for apolar substitutions for the lysine side chain K84 (13–15). The composite view is that ~70% of these alterations do not substantially impact binding to operator DNA, and a similar percentage do not alter binding to inducer IPTG.3 In contrast, the allosteric response to inducer is substantially (and in many cases, dramatically) impacted in ~70% of the proteins examined. Indeed, every position has at least one amino acid substitution with altered allosteric function.

Although there are multiple ways to sort these mutants, we utilized the following allocation (Table 4): Group 1 comprises mutants that have only one inducer/operator binding property that differs from wild-type LacI; Group 2 mutants exhibit increased $[IPTG]_{mid}$, a property that, in part, correlates with diminished allosteric amplitude; Group 3 combine decreased percent operator release *and* decreased allosteric amplitude; and Group 4 mutants have altered operator binding combined with decreases in both operator release and allosteric amplitude. To understand better the mechanism for these changes, we modeled structures for these LacI variants using Pymol (http://pymol.sourceforge.net) (summarized in Table 4, examples in Figure 6). Structures were based on the DNA- and IPTG-bound conformations and on the “mid-state” corresponding to the structure found at intermediate stages in the TMD simulation of the transition from the operator-bound to inducer-bound state of the LacI dimer core (11). Although our deductions from this structural analysis remain simply estimates of the impact of substitutions on the interface, we are nonetheless able to rationalize the effects of these substitutions.

The LacI variants of Group 1 generally comprise substitutions (1) of hydrophobic amino acids with polar, acidic, or bulkier apolar side chains or (2) of the polar residue S97 by an apolar residue. The most striking feature for this set of proteins is varied alteration in protein stability, which primarily correlates with crowding observed in the interface (Table 4).

[3]For both operator and inducer binding, substantial impact is >3-fold difference from wild-type LacI.

In the Group 2 proteins, polar or charged side chains introduced at positions 94–96 increase the midpoint for IPTG release. In V94D, V94N, and V96T, substitution diminishes IPTG binding (12), whereas V94K and V95D exhibit an increased induction ratio without impact on IPTG binding affinity. The latter effects appear due to repulsion between the charged residues in this interface that impedes the allosteric transition (see Figure 6A for V95D). Interestingly, the Group 2 proteins, with the exception of V96T, also exhibit lower urea stability, likely due to disruptions of the apolar network and possible charge-charge repulsion across the subunit interface, as detailed previously for V94D (12).

Group 3 proteins exhibit normal operator affinity, but significantly decreased allosteric amplitude, including a lower level of operator release and lower affinity for inducer (except K84A and V95K). These proteins exhibit wild-type or enhanced stability to urea. Disruption of movement in the N-subdomain interface due to enhanced apolar character (K84A) or to charge interactions (e.g., S97K and V95K, Figure 6B,C) provides a plausible explanation for these results.

In addition to altered IPTG response, Group 4 proteins bind with lower affinity to operator DNA. In V96K (Figure 6D) and M98K (Figure 6E), the altered side chain inserts deeply into the core hydrophobic regions, resulting in steric crowding that may disrupt the interface and misalign the N-terminal DNA binding domains, similar to behavior observed for K84L (31), and charge repulsion may also play a role. Group 3 and 4 proteins demonstrate that adding charge (positive or negative) or removing charge from this region of the N-subdomain interface can be highly disruptive to LacI allosteric response.

One group 4 protein, M98E, exhibits unique biphasic inducer binding with significantly diminished affinity for the second inducer molecule.4 TMD analyses had suggested that M98 transiently stabilizes the K84 side chain in the process of its move to a more solvent-exposed position in the inducer-bound form (11), providing opportunity for M98E•K84′ interaction (Figure 6F). This stabilizing effect may contribute to the separation of subunit IPTG-binding events as well as decreased affinity for second site. Moreover, the mid-point of operator release tracks with the K_d of the second inducer binding event. This result is consistent with our previous work (13) and recent results using a hybrid LacI dimer/chimeric operator system (32) that demonstrate the requirement for two inducer molecules per LacI dimer to release operator DNA.

Allosteric Behavior

Differences in the subunit interface of the LacI N-subdomain for operator-bound *versus* inducer-bound LacI (5,6,9) have been highlighted by network analysis (10). Computational methods to identify “global communication networks” in proteins have demonstrated that in LacI the N-subdomain monomer•monomer interface serves as a primary pathway for allosteric communication and that contact rearrangement is more directly involved in this process compared to other proteins (33). Data from prior studies of this region targeting K84 (13–15) and V94/V96 (12) have also indicated a role for this region in the allosteric process. Changes in the balance and nature of contributions from apolar and electrostatic/polar interactions can alter protein function, even leading to the different specificities among protein homologues or different family members (*e.g.*, 34–40).

The traditional perception of models for allosteric behavior as either concerted or sequential changes in response to ligand binding have evolved to emphasize population shifts and ensembles of both conformations and pathways, in which the particular structural changes

[4]Although IPTG binding behavior is similar to that previously observed for S77L (17), the latter protein does not bind to DNA (presumably due to crowding in the interface that misaligns the DNA binding domains).

are dependent on the nature of the perturbation (41–43). Recent work on the CAP protein and tetracycline repressor has indicated that alterations in protein folding or flexibility, even in the absence of a substantial conformational change, can exert allosteric influence on binding properties (44–47). With this perspective, the range of impacts that a single variation can have on LacI function may derive from a variety of sources: destabilization or enhancement of a particular pathway of structural changes or alterations in conformational dynamics that translate into modified properties. The degree of impediment to allosteric response will necessarily vary depending on the relative importance of a particular structural pathway in the networks involved in this process. Collectively, the results from protein variants at positions 94–98 demonstrate that this specific region is critical to the conformational alterations required for LacI function and cannot be bypassed by another pathway.

These observations are consistent with previous network and computational analysis that identified this interface as a key allosteric pathway (10,11,33). For wild-type LacI, the K84 side chains wedge open the N-subdomain interface to orient the hinge helix and DNA binding domains for optimal binding and also destabilize the surrounding apolar region of the N-subdomain interface. This arrangement creates a system poised for alteration by inducer binding (5,6,10,11) or by mutation of any of its components. Enhancement of charge at most sites or elimination of K84 charge in this region of the N-subdomain interface limits the functional states available to LacI. M98 performs an interesting role that is influenced strongly by introducing charge on this sidechain. In the presence of IPTG, M98 moves to occupy a less solvent-exposed region of the N-subdomain subunit interface (see Figure 1B right), enhancing the apolar network of interactions in this region, consistent with the negative effects of charge at this site.

Conclusion

The side chain- and position-dependent impacts of mutating side chains at positions 94–98 on LacI function derive from altering the interaction network(s) (10,33) among residues composing this interface. The ability to rearrange this N-subdomain monomer•monomer interface is critical to the allosteric transition required for LacI response to inducer, and substitutions that impede this process or shift the balance toward one conformation have deleterious effects on function. Unlike other proteins where multiple, and potentially alternative, allosteric pathways have been identified (*e.g.*, 33,42,43), the current experiments indicate that this region of the LacI N-subdomain interface pathway dominates the network of potential avenues for communication between the inducer and operator sites in LacI.

Acknowledgments

We thank Liskin Swint-Kruse (The University of Kansas Medical Center) for critical feedback, Zhifei Sun and Kevin Kam for assistance with some IPTG binding experiments, Anishika D'Souza and Shirley Liu for help with experiments, and members of the Matthews laboratory for useful discussions.

REFERENCES

1. Wilson CJ, Zhan H, Swint-Kruse L, Matthews KS. The lactose repressor system: Paradigms for regulation, allosteric behavior and protein folding. Cell. Mol. Life Sci. 2007; 64:3–16. [PubMed: 17103112]
2. Matthews KS, Nichols JC. Lactose repressor protein: Functional properties and structure. Prog. Nucleic Acid Res. Mol. Biol. 1997; 58:127–164. [PubMed: 9308365]
3. Matthews KS, Falcon CM, Swint-Kruse L. Relieving repression. Nature Struct. Biol. 2000; 7:184–187. [PubMed: 10700271]

4. Müller-Hill B. Lac repressor and *lac* operator. Prog. Biophys. Mol. Biol. 1975; 30:227–252. [PubMed: 792953]
5. Lewis M, Chang G, Horton NC, Kercher MA, Pace HC, Schumacher MA, Brennan RG, Lu P. Crystal structure of the lactose operon repressor and its complexes with DNA and inducer. Science. 1996; 271:1247–1254. [PubMed: 8638105]
6. Bell CE, Lewis M. A closer view of the conformation of the Lac repressor bound to operator. Nat. Struct. Biol. 2000; 7:209–214. [PubMed: 10700279]
7. Friedman AM, Fischmann TO, Steitz TA. Crystal structure of *lac* repressor core tetramer and its implications for DNA looping. Science. 1995; 268:1721–1727. [PubMed: 7792597]
8. Chen J, Matthews KS. Deletion of lactose repressor carboxyl-terminal domain affects tetramer formation. J. Biol. Chem. 1992; 267:13843–13850. [PubMed: 1629185]
9. Bell CE, Lewis M. The Lac repressor: A second generation of structural and functional studies. Curr. Opin. Struct. Biol. 2001; 11:19–25. [PubMed: 11179887]
10. Swint-Kruse L. Using networks to identify fine structural differences between functionally distinct protein states. Biochemistry. 2004; 43:10886–10895. [PubMed: 15323549]
11. Flynn TC, Swint-Kruse L, Kong Y, Booth C, Matthews KS, Ma J. Allosteric transition pathways in the lactose repressor protein core domains: Asymmetric motions in a homodimer. Protein Sci. 2003; 12:2523–2541. [PubMed: 14573864]
12. Zhan H, Sun Z, Matthews KS. Functional impact of polar and acidic substitutions in the lactose repressor hydrophobic monomer•monomer interface with a buried lysine. Biochemistry. 2009; 48:1305–1314. [PubMed: 19166325]
13. Swint-Kruse L, Zhan H, Matthews KS. Integrated insights from simulation, experiment, and mutational analysis yield new details of LacI function. Biochemistry. 2005; 44:11201–11213. [PubMed: 16101304]
14. Chang W-I, Olson JS, Matthews KS. Lysine 84 is at the subunit interface of *lac* repressor protein. J. Biol. Chem. 1993; 268:17613–17622. [PubMed: 8349640]
15. Nichols JC, Matthews KS. Combinatorial mutations of *lac* repressor: Stability of monomer-monomer interface is increased by apolar substitution at position 84. J. Biol. Chem. 1997; 272:18550–18557. [PubMed: 9228020]
16. Chakerian AE, Pfahl M, Olson JS, Matthews KS. A mutant lactose repressor with altered inducer and operator binding parameters. J. Mol. Biol. 1985; 183:43–51. [PubMed: 3892017]
17. Chou W-Y, Matthews KS. Mutation in hinge region of lactose repressor protein alters physical and functional properties. J. Biol. Chem. 1989; 264:6171–6176. [PubMed: 2703485]
18. Wycuff DR, Matthews KS. Generation of an AraC-*ara*BAD promoter-regulated T7 expression system. Anal. Biochem. 2000; 277:67–73. [PubMed: 10610690]
19. Chen J, Matthews KS. Deletion of lactose repressor carboxyl-terminal domain affects tetramer formation. J. Biol. Chem. 1992; 267:13843–13850. [PubMed: 1629185]
20. Zhan H, Swint-Kruse L, Matthews KS. Extrinsic interactions dominate helical propensity in coupled binding and folding of lactose repressor protein hinge helix. Biochemistry. 2006; 45:5896–5906. [PubMed: 16669632]
21. Wong I, Lohman TM. A double-filter method for nitrocellulose-filter binding: Application to protein-nucleic acid interactions. Proc. Natl. Acad. Sci. U. S. A. 1993; 90:5428–5432. [PubMed: 8516284]
22. Falcon CM, Matthews KS. Engineered disulfide linking the hinge regions within lactose repressor dimer increases operator affinity, decreases sequence selectivity, and alters allostery. Biochemistry. 2001; 40:15650–15659. [PubMed: 11747440]
23. Laiken SL, Gross CA, von Hippel PH. Equilibrium and kinetic studies of *Escherichia coli lac* repressor-inducer interactions. J. Mol. Biol. 1972; 66:143–155. [PubMed: 4557195]
24. Swint-Kruse L, Zhan H, Fairbanks BM, Maheshwari A, Matthews KS. Perturbation from a distance: Mutations that alter LacI function through long-range effects. Biochemistry. 2003; 42:14004–14016. [PubMed: 14636069]
25. Barry JK, Matthews KS. Thermodynamic analysis of unfolding and dissociation in lactose repressor protein. Biochemistry. 1999; 38:6520–6528. [PubMed: 10350470]

26. Chen J, Matthews KS. Subunit dissociation affects DNA binding in a dimeric *lac* repressor produced by C-terminal deletion. Biochemistry. 1994; 33:8728–8735. [PubMed: 8038163]
27. Warren JR, Gordon JA. On the refractive indices of aqueous solutions of urea. J. Phys. Chem. 1966; 70:297–300.
28. Pace CN. Determination and analysis of urea and guanidine hydrochloride denaturation curves. Methods Enzymol. 1986; 131:266–280. [PubMed: 3773761]
29. Santoro MM, Bolen DW. Unfolding free energy changes determined by the linear extrapolation method. 1. Unfolding of phenylmethanesulfonyl α-chymotrypsin using different denaturants. Biochemistry. 1988; 27:8063–8068. [PubMed: 3233195]
30. Suckow J, Markiewicz P, Kleina LG, Miller J, Kisters-Woike B, Müller-Hill B. Genetic studies of the Lac repressor XV: 4000 single amino acid substitutions and analysis of the resulting phenotypes on the basis of the protein structure. J. Mol. Biol. 1996; 261:509–523. [PubMed: 8794873]
31. Bell CE, Barry J, Matthews KS, Lewis M. Structure of a variant of *lac* repressor with increased thermostability and decreased affinity for operator. J. Mol. Biol. 2001; 313:99–109. [PubMed: 11601849]
32. Daber R, Sharp K, Lewis M. One is not enough. J. Mol. Biol. 2009; 392:1133–1144. [PubMed: 19631220]
33. Daily MD, Gray JJ. Allosteric communication occurs via networks of tertiary and quaternary motions in proteins. PLoS Comp. Biol. 2009; 5:1–14. e1000293.
34. Ortiz-Maldonado M, Cole LJ, Dumas SM, Entsch B, Ballou DP. Increased positive electrostatic potential in *p*-hydroxybenzoate hydroxylase accelerates hydroxylation but slows turnover. Biochemistry. 2004; 43:1569–1579. [PubMed: 14769033]
35. Christodoulou E, Rypniewski WR, Vorgias CE. High-resolution X-ray structure of the DNA-binding protein HU from the hyper-thermophilic *Thermotoga maritima* and the determinants of its thermostability. Extremophiles. 2003; 7:111–122. [PubMed: 12664263]
36. Prochnicka-Chalufour A, Casanova J-L, Avrameas S, Claverie J-M, Kourilsky P. Biased amino acid distributions in regions of the T cell receptors and MHC molecules potentially involved in their association. Internatl. Immunol. 1991; 3:853–864.
37. Crowley PB, Ubbink M. Close encounters of the transient kind: Protein interactions in the photosynthetic redox chain investigated by NMR spectroscopy. Acc. Chem. Res. 2003; 36:723–730. [PubMed: 14567705]
38. Díaz-Moreno I, Díaz-Quintana A, De la Rosa MA, Crowley PB, Ubbink M. Different modes of interaction in cyanobacterial complexes of plastocyanin and cytochrome *f*. Biochemistry. 2005; 44:3176–3183. [PubMed: 15736928]
39. Nakajima K, Kato H, Oda J, Yamada Y, Hashimoto T. Site-directed mutagenesis of putative substrate-binding residues reveals a mechanism controlling the different stereospecificities of two tropinone reductases. J. Biol. Chem. 1999; 274:16563–16568. [PubMed: 10347221]
40. Sakaguchi M, Tomiyoshi R, Kuroiwa T, Mihara K, Omura T. Functions of signal and signal-anchor sequences are determined by the balance between the hydrophobic segment and the N-terminal charge. Proc. Natl. Acad. Sci. U. S. A. 1992; 89:16–19. [PubMed: 1729684]
41. Cui Q, Karplus M. Allostery and cooperativity revisited. Protein Sci. 2008; 17:1295–1307. [PubMed: 18560010]
42. Hilser VJ. An ensemble view of allostery. Science. 2010; 327:653–654. [PubMed: 20133562]
43. del Sol A, Tsai CJ, Ma B, Nussinov R. The origin of allosteric functional modulation: Multiple pre-existing pathways. Structure. 2009; 17:1042–1050. [PubMed: 19679084]
44. Tzeng S-R, Kalodimos CG. Dynamic activation of an allosteric regulatory protein. Nature. 2009; 462:368–374. [PubMed: 19924217]
45. Beckett D. Regulating transcription regulators via allostery and flexibility. Proc. Natl. Acad. Sci. U. S. A. 2009; 106:22035–22036. [PubMed: 20080782]
46. Reichheld SE, Zhou Y, Davidson AR. The induction of folding cooperativity by ligand binding drives the allosteric response of tetracycline repressor. Proc. Natl. Acad. Sci. U. S. A. 2009; 106:22263–22268. [PubMed: 20080791]

47. Toncrova H, McLeish TC. Substrate-modulated thermal fluctuations affect long-range allosteric signaling in protein homodimers: Exemplified in CAP. Biophys. J. 2010; 98:2317–2326. [PubMed: 20483341]

48. Pettersen EF, Goddard TD, Huang CC, Couch GS, Greenblatt DM, Meng EC, Ferrin TE. UCSF Chimera — A visualization system for exploratory research and analysis. J. Comput. Chem. 2004; 25:1605–1612. [PubMed: 15264254]

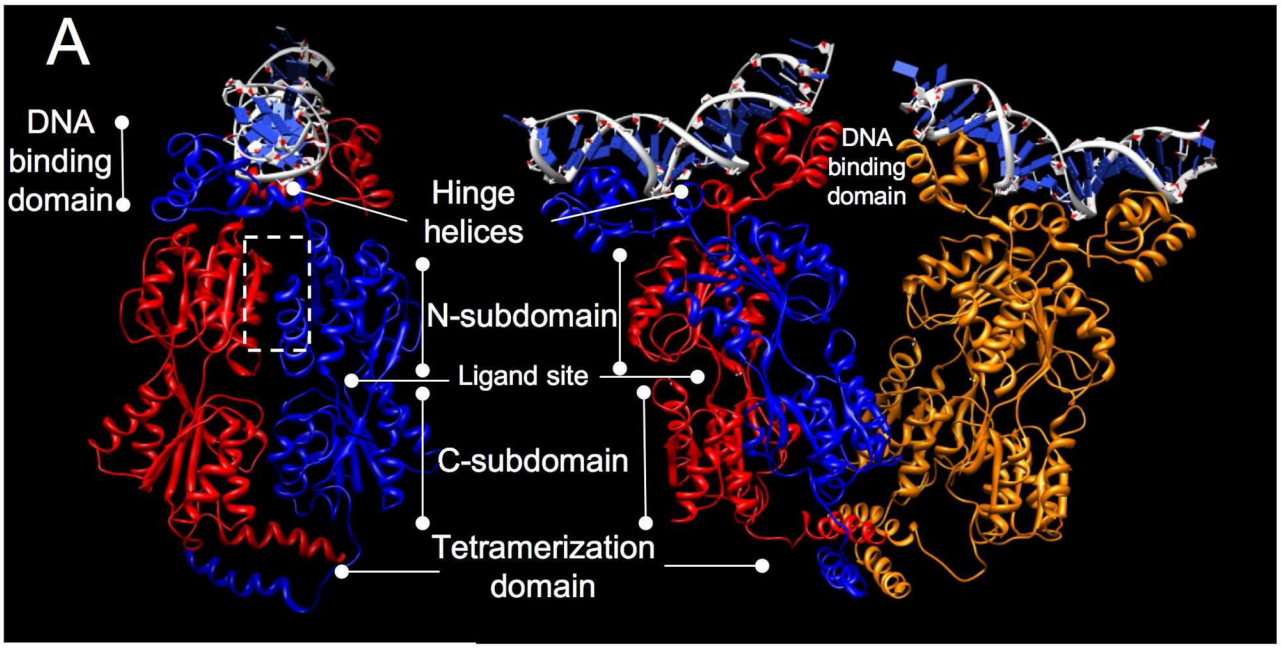

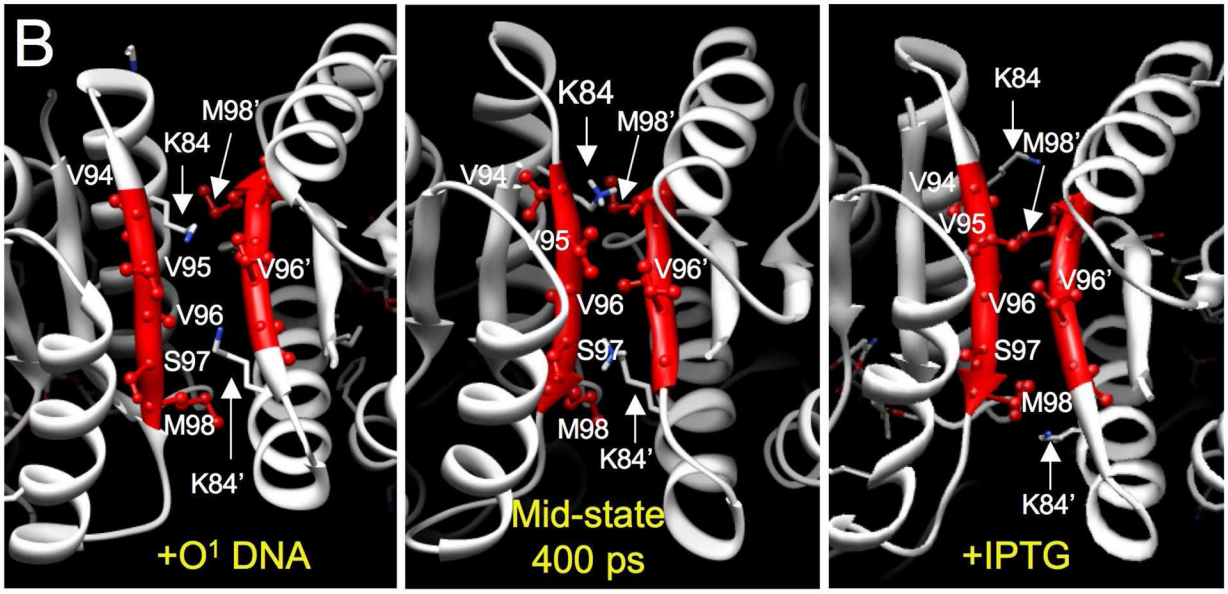

Figure 1.

(A) The structure of LacI is shown as dimer (left) and tetramer (right) in operator DNA-bound form (5) (coordinates from Protein Data Bank file 1lbg). The ONPF ligand is not shown. The two monomers are colored differently within the dimer alone and in the left dimer of the tetramer. The domains found within each monomer are indicated in the figure: N-terminal DNA binding domain, hinge helices, N- and C-subdomains of the core domain with the ligand-binding site between, and the C-terminal tetramerization domain. (B) Enlarged views of the N-subdomain monomer•monomer interface from the perspective of the DNA binding domain (area shown outlined approximately by dashed line in Panel A, left). Changes in this region occur between the different states: DNA-bound (left, PDB file

lefa (6)), mid-state of targeted molecular dynamics transition at 400 ps (center, (11)), and inducer-bound (right, PDB file 1lbh (5)). [Note that time is artificial in the TMD analysis, but allows correlation with information in ref 11.] Side chains targeted in this study and K84 are labeled on the left strand; right strand residues K84′, V96′ and M98′ are labeled for orientation. Note that the interface surrounding K84 undergoes major rearrangements in response to inducer binding (see text). Molecular graphics images were produced using the UCSF Chimera package (http://www.cgl.ucsf.edu/chimera) from the Resource for Biocomputing, Visualization, and Informatics at the University of California, San Francisco (supported by NIH P41 RR-01081) (48).

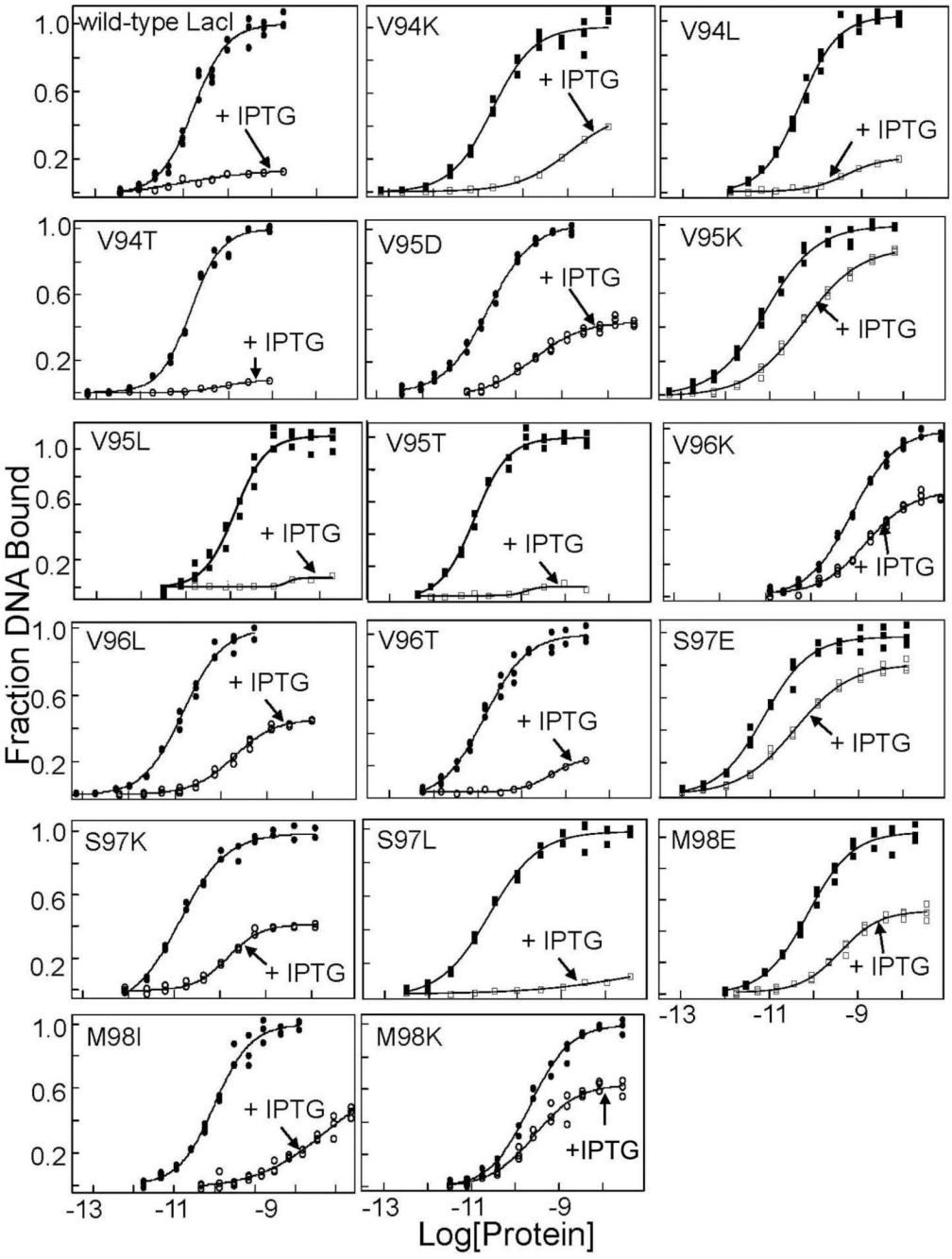

Figure 2.

DNA (O^1) binding in the absence and presence of inducer for wild-type LacI and the mutant proteins. Experiments were conducted in buffer containing 0.01 M Tris-HCl, pH 7.4, 0.15 M KCl, 0.3 mM DTT, 0.1 mM EDTA, 5% DMSO, and 100 μg/ml bovine serum albumin in the absence (filled circles) or presence (open circles) of IPTG as described in Materials and Methods. The DNA concentration was below 1.5×10^{-12} M, and, where present, IPTG concentration was 1 mM. Data shown are for single determinations (with triplicate points), and the results from multiple determinations are summarized in Table 1. For a subset of proteins (*e.g.*, V95D, V95K, V96K, V96L, S97E, S97K, M98E, M98K), substantial binding to operator in the presence of IPTG is observed. The lower saturation value in the presence

of IPTG may indicate that the kinetics of the reaction differ from wild-type LacI; no kinetic measurements were pursued to address this issue.

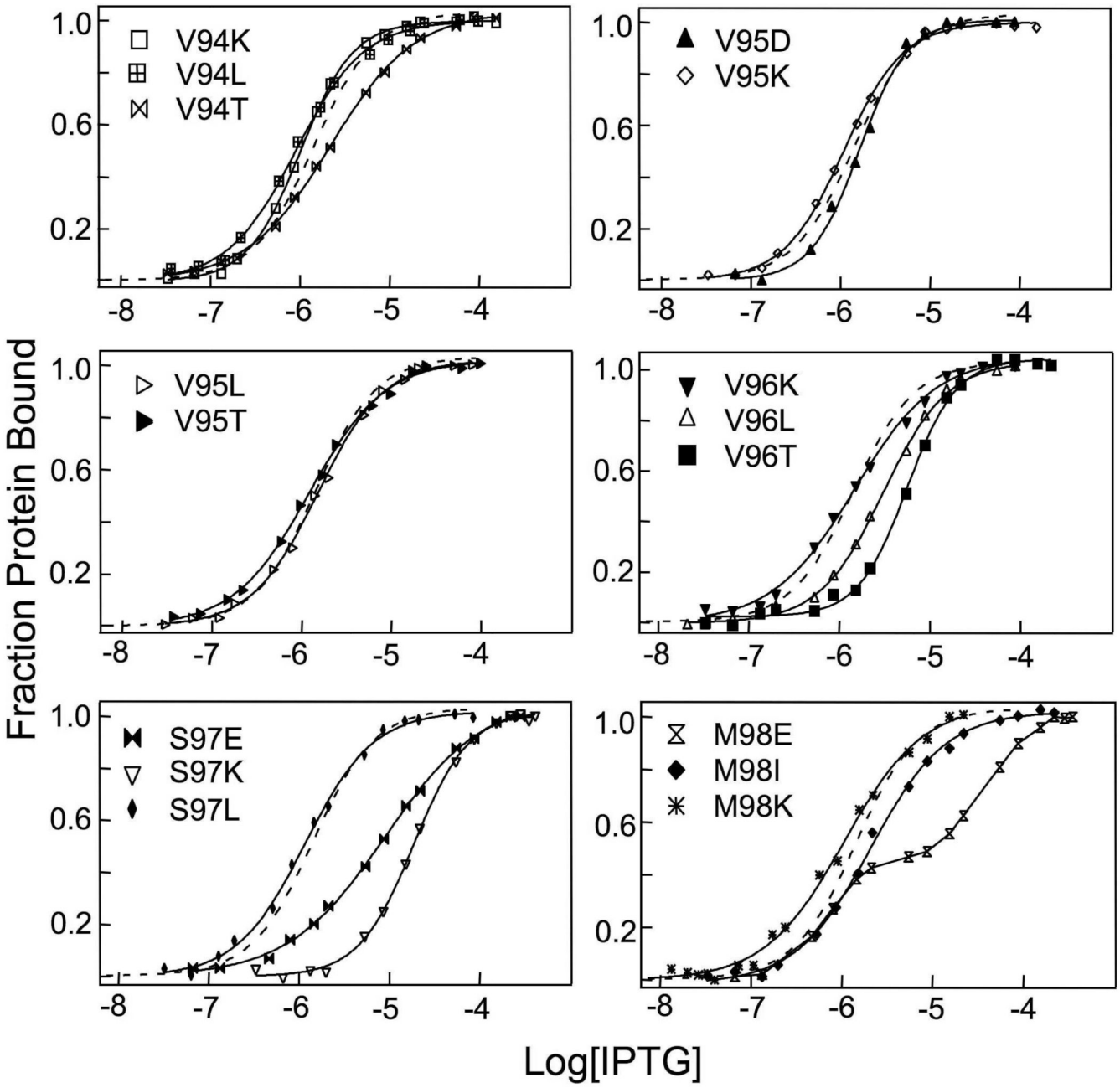

Figure 3.

IPTG binding of wild-type LacI and interface mutants. Buffer was 0.01 M Tris-HCl, pH 7.4, 0.15 M KCl. The experiments were conducted as described in Materials and Methods. Data are shown for single determinations, and the results from multiple determinations are summarized in Table 2. The data for wild-type LacI are shown as a dotted line for comparison in each panel.

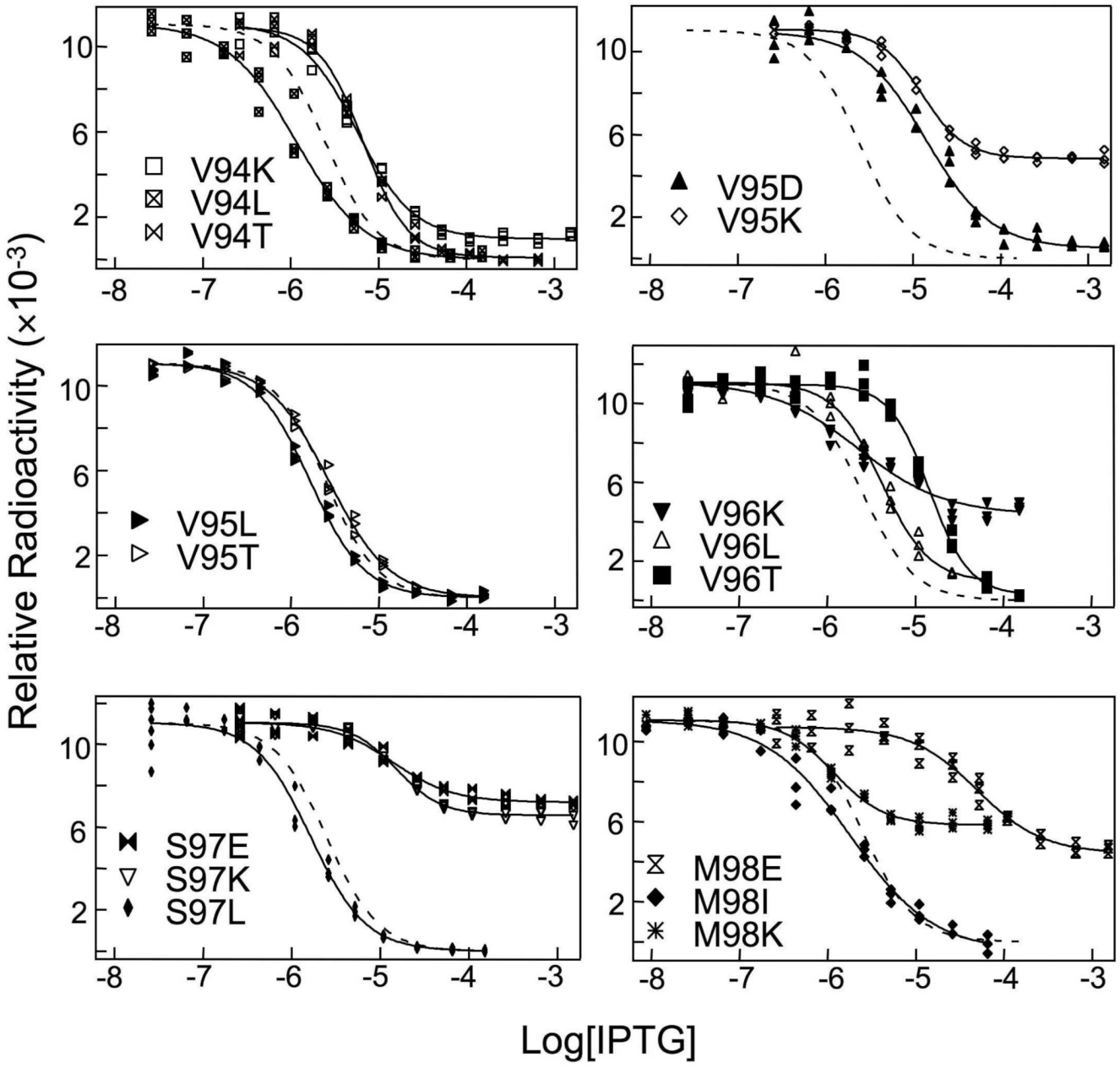

Figure 4.

Operator release by IPTG for wild-type LacI and interface variants. The experiments were performed as described in Materials and Methods in buffer containing 0.01 M Tris-HCl, pH 7.4, 0.15 M KCl, 0.3 mM DTT, 0.1 mM EDTA, 5% DMSO, and 100 μg/ml bovine serum albumin with the indicated concentrations of IPTG. Operator concentration was 1.5×10^{-12} M, and protein concentrations were as indicated in Materials and Methods. Data for a single experiment are shown (triplicate points), and the results from multiple measurements are summarized in Table 2. The data for wild-type LacI are shown as a dotted line for comparison in each panel.

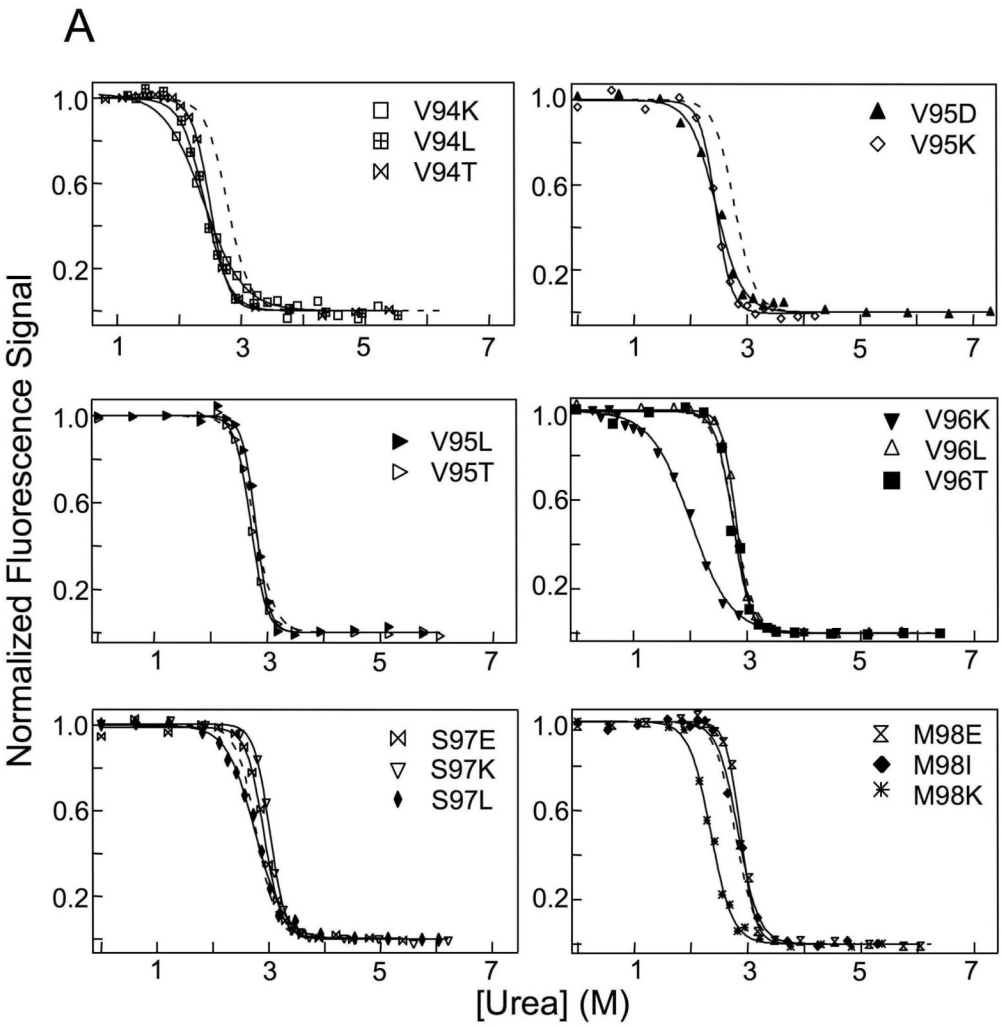

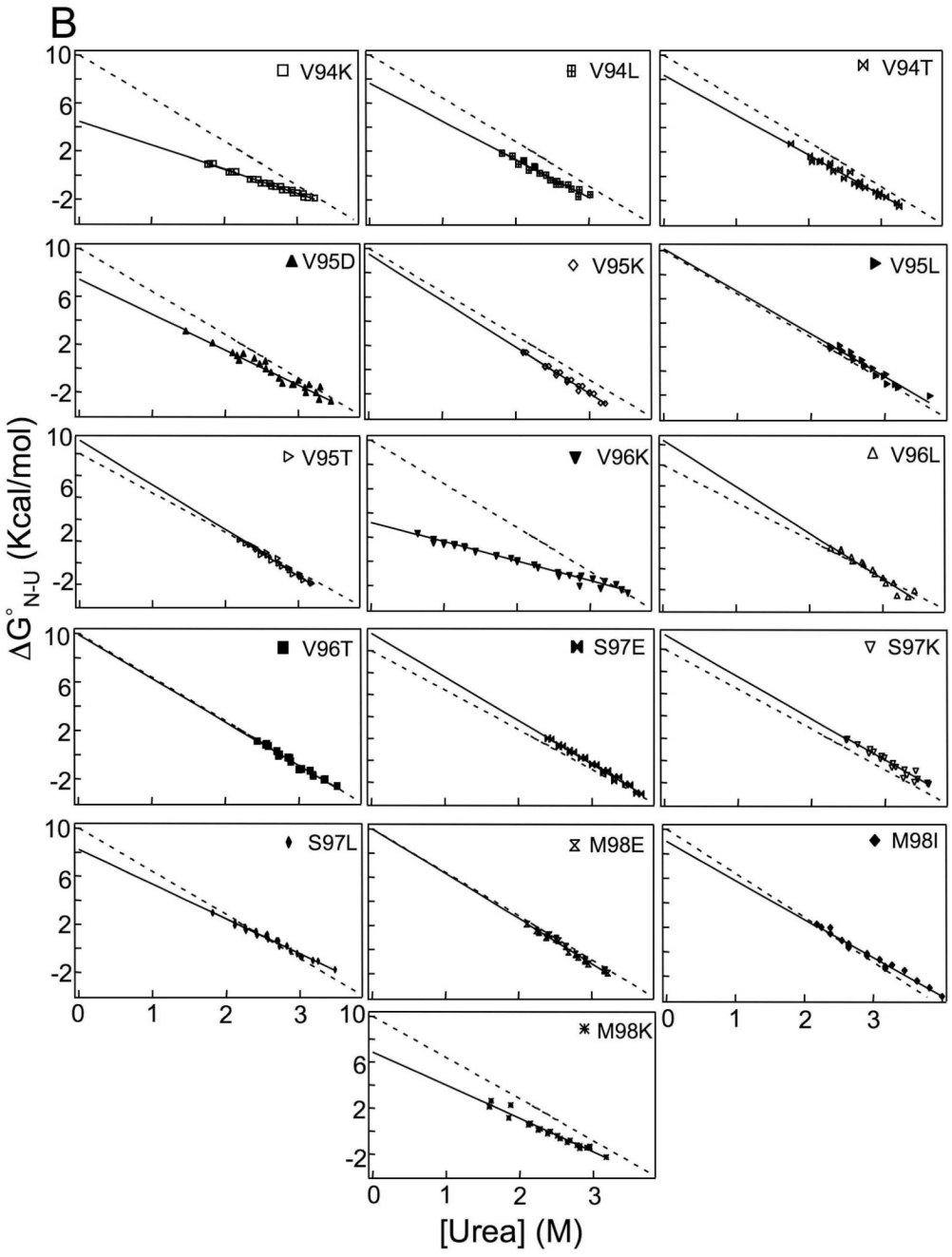

Figure 5.

Urea denaturation of wild-type LacI and interface mutant proteins. The experiments were conducted as previously described (12,20) in buffer containing 0.01 M Tris-HCl, pH 7.5, 0.1 M K_2SO_4. Protein concentration was 2×10^{-6} M in monomer. (A) Fluorescence measurements of denaturation were used to determine the mid-point values reported for multiple experiments in Table 3. The data for wild-type LacI are shown as a dotted line for comparison in each panel. (B) Global fits for the denaturation data are shown for wild-type LacI and protein variants. Fluorescence data, and in some instances circular dichroism data, were utilized in determining the unfolding free energy (energy ($\Delta G°_{N-U}$) and *m* values. Data

analysis utilized linear extrapolation to zero urea to calculate the $\Delta G°_{N\text{-}U}$ (28). A dashed line in each panel represents the fit for wild-type LacI data for comparison.

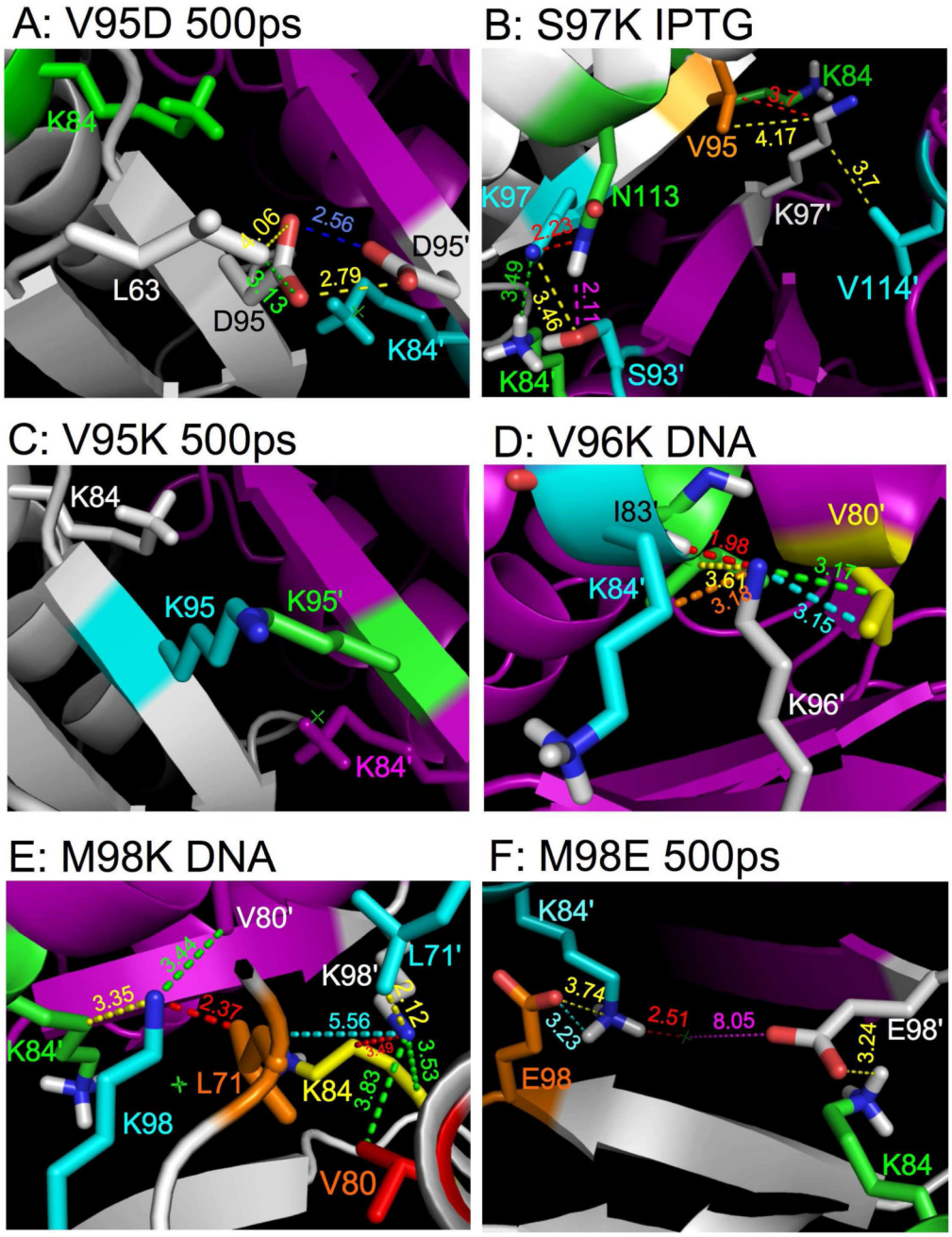

Figure 6.

N-subdomain monomer•monomer interface structures of variant proteins. These structures for LacI mutant proteins were generated using the mutagenesis function in PyMol (http://pymol.sourceforge.net) using DNA-bound LacI (Protein Data Bank entry 1efa) (6), IPTG-bound LacI (Protein Data Bank Entry 1lbh) (5), or an intermediate in the TMD-generated pathway (11). Where relevant, distances are shown with labeled dashed lines, and numbers with the lines are the distances in Ångstroms. (A) The close apposition required for V95D/V95D′ negatively charged side chains in the intermediate found at 500 ps in the TMD simulation would impede the allosteric transition (11). (B) In S97K, charge repulsion occurs between the introduced lysine and K84′ in the IPTG-bound form (shown in Panel B) as well

as in the intermediate structure. (C) Charge repulsion between K95 and K95′ impedes the allosteric transition for V95K, as seen in the intermediate structure at 500 ps of the TMD simulation. (D,E) The charged side chains of V96K (Panel D) or M98K (Panel E) invade the hydrophobic region surrounding the subunit interface, generating significant steric crowding that impacts DNA binding as well as charge interactions that destabilize these mutant proteins and preclude response to inducer. (F) Formation of an ion-pair between the charged side chain of M98E and that of K84′ at 500 ps in the TMD model for the transition fixes and distorts the subunit interface, providing an explanation for alterations in both DNA and IPTG affinity and the observed impediment to binding of the second inducer.

Table 1

Operator O^1 binding properties and inducibility of interface variants[a,b]

	$K_{R/O}$ ($M \times 10^{-11}$)	Ratio $K_{R/O\ mutant}/K_{R/O\ WT}$	$K_{RI/O}$[c] ($M \times 10^{-11}$)	$K_{RI/O}/K_{R/O}$ Allosteric amplitude	Phenotype[d]
WTLacI	1.5 ± 0.4		>10000	>1000	+
V94K	2.0 ± 0.1	1.3 ± 0.4	>1000	>100	−
V94L	4.0 ± 1	2.7 ± 0.7	>10000	>1000	+ws
V94T	1.3 ± 0.1	0.90 ± 0.1	>10000	>1000	NDA[e]
V95D	3.1 ± 0.4	2.1 ± 0.2	26 ± 2	8.4 ± 1.0	NDA
V95K	0.73 ± 0.08	0.49 ± 0.2	6.0 ± 0.4	8.2 ± 0.9	+ s
V95L	12 ± 2	8.0 ± 2	>10000	>800	+−
V95T	0.90 ± 0.07	0.60 ± 0.2	>10000	>1000	NDA
V96K	89 ± 9	60 ± 8	170 ± 10	1.9 ± 0.2	+ s
V96L	0.90 ± 0.6	0.60 ± 0.4	17 ± 9	19 ± 2	+ s
V96T	1.4 ± 0.4	0.93 ± 0.3	>10000	>1000	NDA
S97E	0.65 ± 0.09	0.43 ± 0.2	3.7 ± 0.2	5.7 ± 0.8	+ s
S97K	1.3 ± 0.2	0.87 ± 0.2	13 ± 5	10 ± 2	+ s
S97L	2.4 ± 0.1	1.6 ± 0.4	>10000	>1000	+
M98E	7.6 ± 0.7	5.1 ± 1	44 ± 7	5.8 ± 0.6	+−ws
M98I	10 ± 2	6.7 ± 2	>1000	>100	NDA
M98K	21 ± 2	14 ± 3	31 ± 4	1.5 ± 0.2	−

[a] Standard deviations shown represent a minimum of 3 measurements and up to 5 measurements.

[b] Operator binding experiments were performed in buffer containing 0.01 M Tris-HCl, pH 7.4, 0.15 M KCl, 0.3 mM DTT, 0.1 mM EDTA, 5% DMSO, and 100 μg/ml bovine serum albumin.

[c] For O^1 binding with IPTG, operator concentration was below 1.5×10^{-12} M.

[d] Data from Suckow *et al.* (30): +, repression > 200-fold; -, repression < 5-fold; S, I^S phenotype (insensitive to inducer); ws, weak I^S phenotype.

[e] NDA: no data available.

Table 2

Inducer-binding properties of interface mutants[a]

	$K_{R/I}(M \times 10^6)$[b]	$[IPTG]_{mid}$ $(M \times 10^6)$ operator release[c]	Ratio for $[IPTG]_{mid}$ mutant/WT	Relative % operator release[d]	Induction Ratio[e] $[IPTG]_{mid}/ K_{R/I}$
WTLacI	1.2 ± 0.1	2.9 ± 0.6		100	2.4 ± 0.3
V94K	1.1 ± 0.1	5.5 ± 0.2	1.9 ± 0.4	95	5.0 ± 0.5
V94L	0.90 ± 0.08	1.2 ± 0.1	0.41 ± 0.1	100	1.3 ± 0.1
V94T	2.6 ± 0.3	8.0 ± 0.6	2.8 ± 0.3	99	3.1 ± 0.4
V95D	1.7 ± 0.1	14 ± 2	4.8 ± 2	96	8.2 ± 1
V95K	1.1 ± 0.1	11 ± 1	3.8 ± 0.8	56	10 ± 1
V95L	1.2 ± 0.1	1.6 ± 0.1	0.55 ± 0.1	100	1.3 ± 0.3
V95T	1.5 ± 0.2	2.7 ± 0.4	0.93 ± 0.2	100	1.8 ± 0.3
V96K	1.3 ± 0.1	2.6 ± 0.6	0.90 ± 0.2	61	2.0 ± 0.3
V96L	3.3 ± 0.4	5.0 ± 0.5	1.7 ± 0.2	91	1.5 ± 0.2
V96T	6.0 ± 0.4	18 ± 4	6.2 ± 1	98	3.0 ± 0.2
S97E	8.9 ± 0.3	15 ± 0.3	5.2 ± 1	35	1.7 ± 0.1
S97K	17 ± 2	43 ± 2	15 ± 3	41	2.5 ± 0.3
S97L	1.2 ± 0.1	1.7 ± 0.3	0.59 ± 0.2	100	1.4 ± 0.2
M98E	0.91±0.2/38±10	52 ± 2	18 ± 4	57	[57/1.4]
M98I	2.7 ± 0.4	2.3 ± 0.5	0.80 ± 0.3	100	0.9 ± 0.2
M98K	1.3 ± 0.2	1.1 ± 0.1	0.38 ± 0.1	47	0.9 ± 0.2

[a] Values shown represent a minimum of 3 measurements and up to 6 measurements.

[b] IPTG binding experiments were conducted in buffer containing 0.01 M Tris-HCl, pH 7.4, 0.15 M KCl.

[c] Operator release experiments were performed in buffer containing 0.01 M Tris-HCl, pH 7.4, 0.15 M KCl, 0.3 mM DTT, 0.1 mM EDTA, 5% DMSO, and 100 μg/ml bovine serum albumin. Protein concentration was as indicated in Materials and Methods.

[d] This ratio is equal to amount of released operator over amount of total amount of operator in the complex.

[e] The induction ratio is the IPTG concentration at the mid-point of operator release ($[IPTG]_{mid}$) divided by the K_d for repressor-IPTG ($K_{R/I}$).

Table 3

Unfolding of interface variants[a]

	$[urea]_{mid}$[b]	$\Delta G°_{N-U}$	m
WTLacI	2.8 ± 0.1	10 ± 0.6	3.6 ± 0.2
V94K	2.2 ± 0.1	4.5 ± 0.1	2.0 ± 0.1
V94L	2.4 ± 0.1	7.7 ± 0.4	3.2 ± 0.2
V94T	2.5 ± 0.1	8.3 ± 0.3	3.3 ± 0.1
V95D	2.5 ± 0.1	7.4 ± 0.4	2.9 ± 0.1
V95K	2.5 ± 0.1	9.5 ± 0.3	3.8 ± 0.1
V95L	2.9 ± 0.1	10.1 ± 0.5	3.5 ± 0.2
V95T	2.7 ± 0.1	11.0 ± 0.3	4.1 ± 0.1
V96K	2.0 ± 0.1	3.2 ± 0.1	1.6 ± 0.1
V96L	2.8 ± 0.1	12 ± 0.8	4.5 ± 0.3
V96T	2.8 ± 0.1	9.9 ± 0.4	3.6 ± 0.1
S97E	2.9 ± 0.1	11.6 ± 0.3	4.0 ± 0.1
S97K	3.0 ± 0.1	11 ± 0.6	3.8 ± 0.2
S97L	2.8 ± 0.1	8.2 ± 0.2	2.9 ± 0.1
M98E	2.9 ± 0.1	10 ± 0.3	3.7 ± 0.1
M98I	2.8 ± 0.1	9.0 ± 0.3	3.2 ± 0.1
M98K	2.3 ± 0.1	6.9 ± 0.4	2.9 ± 0.1
K84A [c]	>6 M	-	-
K84L [c]	>6 M	-	-

[a] Values shown represent a minimum of 3 measurements and up to 5 measurements.

[b] Urea experiments were performed in buffer containing 0.01 M Tris-HCl, pH 7.5, 0.15 M K_2SO_4. Urea solution was made fresh daily.

[c] K84A and K84L are shown for comparison. For these variants, the unfolding transition is not complete even at 8 M urea; therefore, the $[urea]_{mid}$ cannot be estimated accurately. Data were taken from ref 15.

Table 4

Properties by Protein Groups[a]

Group	Protein	Substitution character	Operator binding affinity	IPTG binding affinity	Allosteric amplitude	$[IPTG]_{mid}$ operator release; % release	Induction Ratio $[IPTG]_{mid}/K_{R/I}$	Urea stability	Structural rationale for effects of substitution at subunit interface[e]
1	**V94E** [b]	Acidic	~	~	~	~	~	↓	Polar addition destabilizes interface
	V94L	Apolar	~	~	~	~	~	↓	Side-chain crowding destabilizes interface
	V94Q [b]	Hydrophilic	~	~	~	~	~	↓	Polar addition destabilizes interface
	V95L	Apolar	↓	~	~	~	~	~	Crowding of subunit interface misaligns N-terminus
	V95T	Polar	~	~	~	~	~	~	No impact
	V96L	Apolar	~	~	↓	~	~	↑	Side-chain crowding distorts/stabilizes interface
	V96N [b]	Polar	~	~	~	~	~	↓↓	Side-chain crowding destabilizes interface
	V96Q [b]	Polar	~	~	↓	~	~	↓↓	Side-chain crowding destabilizes interface
	S97L	Apolar	~	~	~	~	~	↓	Side-chain crowding destabilizes interface
	M98I	Apolar	↓	~	~	~	~	~	Crowding of subunit interface misaligns N-terminus
2	**V94D** [b]	Acidic	~	↓	↓	↑↑	~	↓↓	Diminished apolar interface/rearrangements
	V94K	Basic	~	~	~	↑	↑	↓↓	Charge repulsion in interface and blocked transition
	V94N [b]	Polar	~	↓	↓	↑↑	~	↓	Diminished apolar interface/rearrangements
	V94T	Polar	~	~	~	↑	~	↓	Polar addition disrupts/rearranges interface
	V95D	Acidic	~	~	↓↓	↑	↑↑	↓	Charge repulsion in interface and blocked transition
	V96T	Polar	~	↓	~	↑	~	~	IPTG-state destabilized by apolar/polar clash
3	**K84A** [c]	Apolar	~	~	↓↓	~, ↓%	~	↑↑	Increased apolar interface, loss of K84 “toggle”
	V95K	Basic	~	~	↓↓	↑; ↓%	↑↑	~	Charge-charge impediment to conformational transition
	V96D [b]	Acidic	~	↓↓	↓↓↓	↑↑↑; ↓↓↓%	~	~	Charge relay system fixes interface
	V96E [b]	Acidic	~	↓↓	↓↓↓	↑↑↑; ↓↓↓%	↑	~	Charge relay system fixes interface
	S97E	Acidic	~	↓	↓↓	↑; ↓↓%	~	↑	Impediment to transition/polar network stabilizes interface
	S97K	Basic	~	↓	↓↓	↑↑; ↓↓%	~	~	Charge repulsion between S97K/K84′ “fixes” interface
4	**K84L** [c]	Apolar	↓	~	↓↓	~, ↓%	~	↑↑	See K84A + side chain crowding to misalign N-termini

Group	Protein	Substitution character	Operator binding affinity	IPTG binding affinity	Allosteric amplitude	$[IPTG]_{mid}$ operator release; % release	Induction Ratio $[IPTG]_{mid}/K_{R/I}$	Urea stability	Structural rationale for effects of substitution at subunit interface[e]
	V96K	Basic	↓↓	~	↓↓↓	~; ↓%	~	↓↓	Charge repulsion in interface and conformational transition
	M98E [d]	Acidic	↓	~/↓↓	↓↓	↑↑; ↓%	~	~	Charge interactions M98E/K84′ stabilize intermediate state
	M98K	Basic	↓	~	↓↓↓	~; ↓%	~	↓	Charge repulsion in interface and conformational transition

[a] Collated data from Table 1 to Table 3 and from ref 12–15, with variants grouped as described in the text.

[b] Data from ref 12.

[c] Data from from ref 14,15.

[d] Binding to inducer is biphasic for M98E; the first event appears similar to wild-type LacI binding, but release of operator DNA is correlated with the second binding event.

[e] The mutagenesis function in the program Pymol was utilized to generate models of the subunit interface in different conformations for the mutations. Using the simple annealing simulation to avoid steric clashes, the impact on structure was deduced. Where multiple configurations were present, the model with the higher probability was utilized in this analysis.